Electronic Supplementary Material (ESI) for Nanoscale Horizons.

Electronic Supplementary Information

Tailoring giant quantum transport anisotropy in nanoporous graphenes under electrostatic disorder

Isaac Alcón[1]*, Aron Cummings[1]* and Stephan Roche[1,2]

[1]*Catalan Institute of Nanoscience and Nanotechnology (ICN2), CSIC and BIST, Campus UAB, Bellaterra, 08193 Barcelona, Spain*

[2]*ICREA, Institució Catalana de Recerca i Estudis Avançats, 08070 Barcelona, Spain*

*Corresponding authors: isaac.alcon@icn2.cat, aron.cummings@icn2.cat

Methods

The unit cells shown in Fig. 1 were used to construct first nearest-neighbour TB models with parameters generally utilized for graphene (t_{ij} = -2.7 eV, ε_0 = 0 eV). The band structures for each material were generated with the Python-based SISL utility.[1] Unit cells were repeated along the *x* and *y* directions to obtain 300x300 nm^2 samples for each material (see Table 1). LSQT simulations are based on the Chebyshev polynomial expansion,[2] which in our case used 4000 moments and an energy broadening of 0.02 eV. For the pristine systems, each material was calculated using ten different initial random phases, thus obtaining statistically averaged quantities. Different time steps were used for the different plots of Fig. 1, ranging from 0.05 to 2 fs.

For the samples including disorder, we considered ten random puddle distributions of the form shown in Eq. 7. In order to speed up the Hamiltonian construction, we imposed a cutoff of the Gaussian tail at 6β (Eq. 7), thus neglecting on-site modifications, ε_i, lower than $4 \cdot 10^{-8}$ eV. For each puddle distribution we ran ten initial random phase distributions, thus effectively averaging over 100 LSQT runs per material, which allowed us to significantly reduce the noise of the different calculated quantities.

Section S1: Ballistic transport at $E - E_F = 0.7$ eV

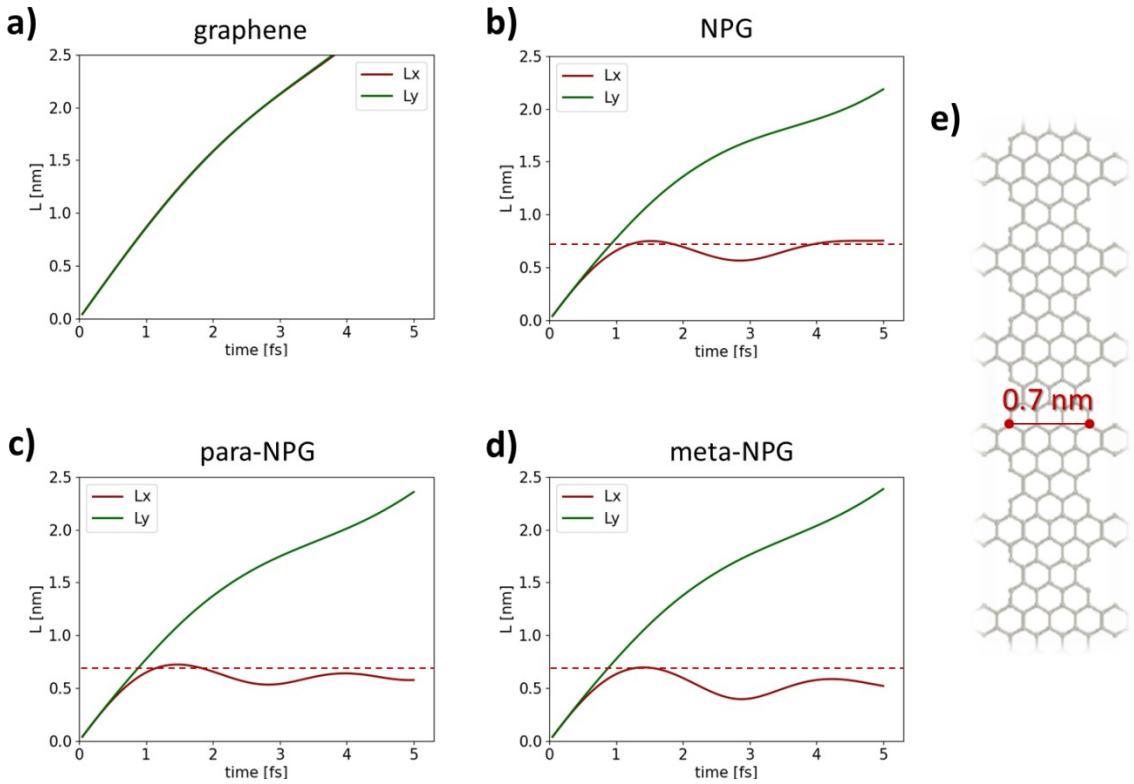

Fig. S1. Wave packet propagation length computed for the first 5 fs along the direction parallel to GNRs (L_y, green curves) and perpendicular to them (L_x, red curves) for a) graphene, b) NPG, c) para-NPG and d) meta-NPG in the pristine form. Red dotted lines indicate the average width of the 7-13-AGNR composing these NPGs, as highlighted in e).

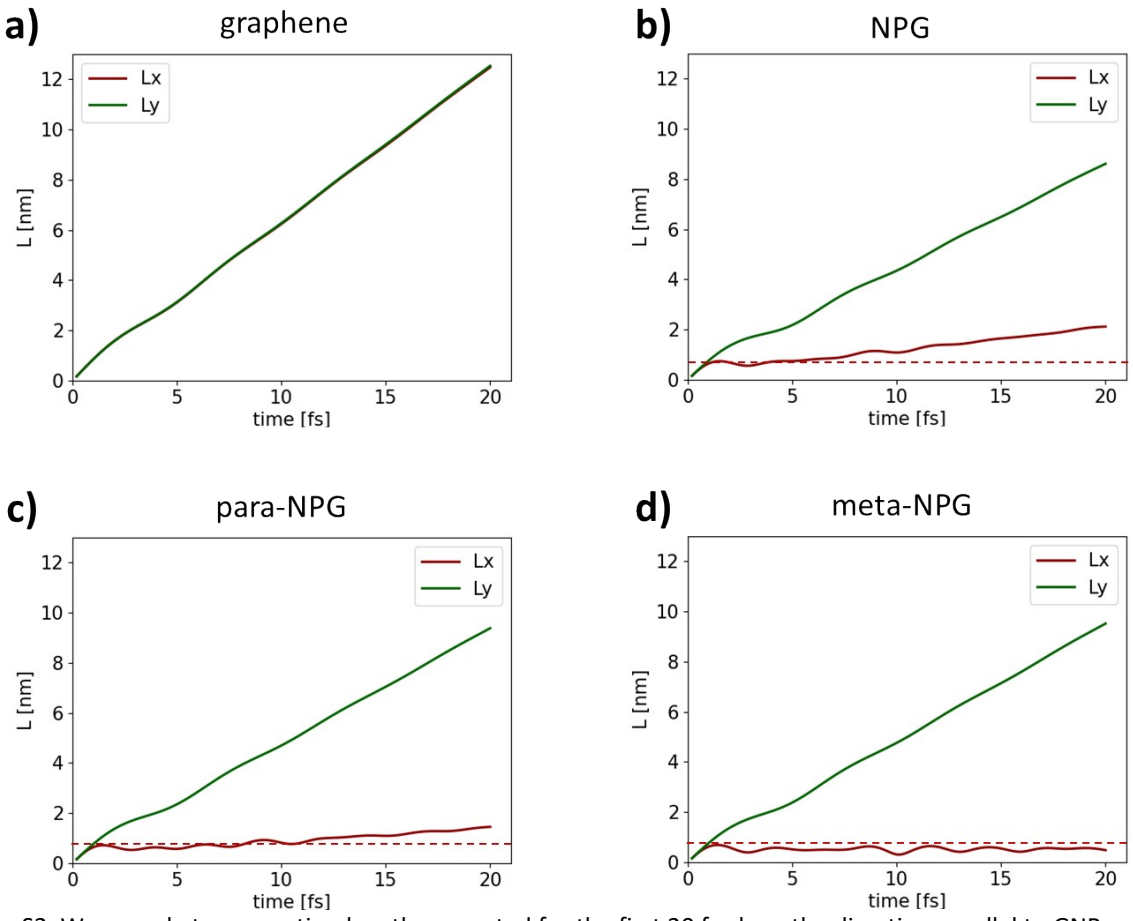

Fig. S2. Wave packet propagation length computed for the first 20 fs along the direction parallel to GNRs (L_y, green curves) and perpendicular to them (L_x, red curves) for a) graphene, b) NPG, c) para-NPG and d) meta-NPG in the pristine form. Red dotted lines indicate the average width of the 7-13-AGNR composing these NPGs, as depicted in Fig. S1.

Table S1. Transport anisotropy values at E – E_F = 0.7 eV for each considered material in the pristine form.

	graphene	NPG	para-NPG	meta-NPG
$A = \bar{v}_y/\bar{v}_x$	1.0	6.0	8.6	71.7

Section S2: Characterization of strong localization in NPGs

For situations where scattering strongly affects transport (normally in highly disordered systems) the transport regime may evolve from diffusive to weakly or strongly localized.[2] The weak localization regime is characterized by a slowly decaying conductivity with length, following the relation

$$\sigma_{WL}(L) = \sigma_{sc} - \frac{2e^2}{\pi h} ln\left(\frac{L}{L_{sc}}\right), \quad \text{Eq. (S1)}$$

where σ_{sc} is the semi-classical conductivity (maximum of the curve), *e* is the elementary charge, *h* is Planck's constant, *L* is the wave-packet length along the transport direction and L_{sc} is the

length at which the conductivity equals σ_{sc}. In Fig. S3 we plot $\sigma_y(L_y)$ for the NPG and para-NPG under electrostatic disorder (see main text for details) along with the weak localization prediction for each case using Eq. S1.

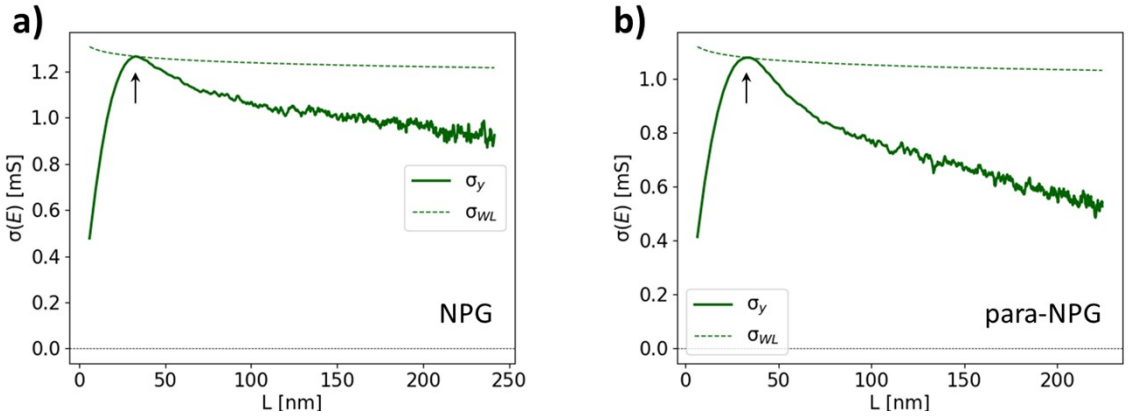

Fig. S3. Conductivity along the GNR direction (σ_y; continuous lines) and its weak localization estimate (σ_{WL}; dotted lines) for a) NPG and b) para-NPG at E – E_F = 0.4eV. σ_{WL} is obtained from the semi-classical conductivity (σ_y^{sc}; see arrows) using equation S1. For further details see section 5.4 in the LSQT review article.[2] Note that meta-NPG has not been included due to its strongly decaying $\sigma_y(L_y)$ well beyond the weak localization tendency.

As one can see, $\sigma_y(L_y)$ decays more strongly in both the NPG and para-NPG than σ_{WL}, indicating that all NPGs should be in the strong localization regime under the considered disorder profile. Strong localization is characterized by an exponentially decaying conductance with increasing wave packet length.[2] At a given energy, the conductance may be obtained from the conductivity as

Eq. (S2) $$G(L) = \sigma(L)\frac{W}{L},$$

where *L* and *W* are the propagated length and width of the wave-packet and, hence, for each in-plane transport direction we get

Eq. (S3) $$G_y(L_y) = \sigma_y(L_y)\frac{L_x}{L_y} \quad ; \quad G_x(L_x) = \sigma_x(L_x)\frac{L_y}{L_x}.$$

For each in-plane direction, in the strong localization regime the conductance is expected to decrease according to

Eq. (S4) $$G(E,L) \propto exp[-L/\xi(E)],$$

where $\xi(E)$ is the localization length, characteristic of this regime, which provides access to the saturated propagation length ($L_{t=\infty}$),

Eq. (S5) $$L_{t=\infty}(E) = \pi \cdot \xi(E).$$

Figs. S4-6 depict $G_y(L_y)$ and $G_x(L_x)$ and the corresponding exponential fits restricted to the highlighted regions of each plot. The good correspondence between the fits and the calculated data confirms the presence of strong localization along both in-plane directions in all NPGs.

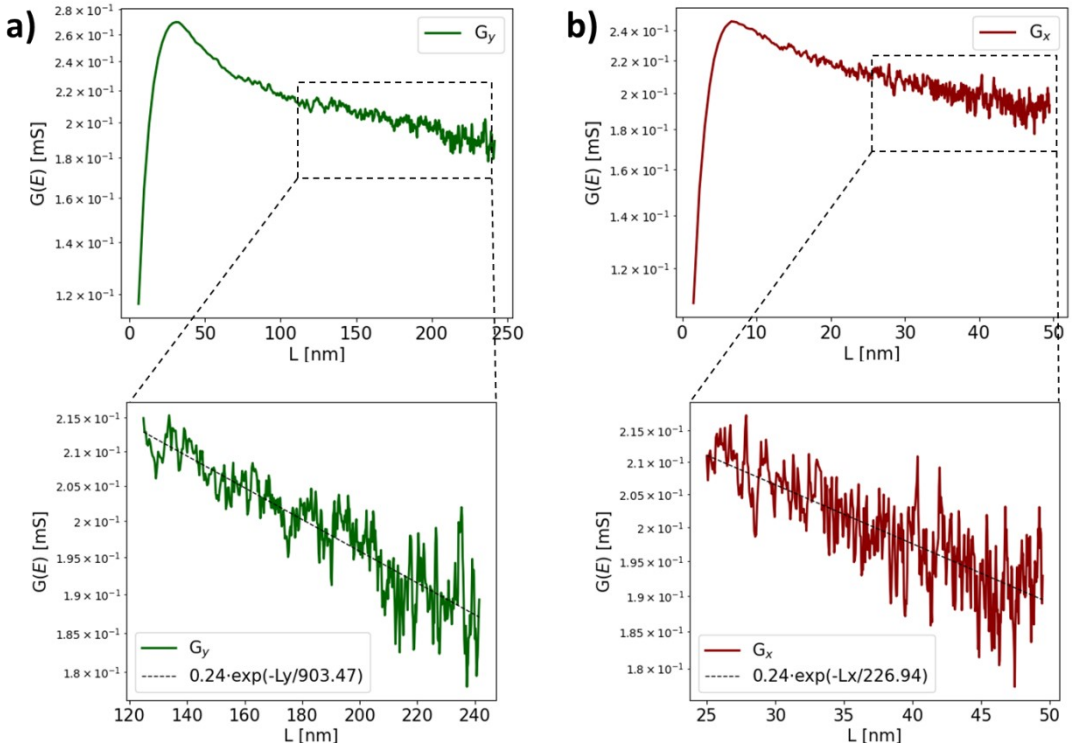

Fig. S4. a) Log-scale plots of $G_y(L_y)$ and b) $G_x(L_x)$ for the NPG at E – E_F = 0.4eV and their fit to an exponential decay. Such fitting provides access to the localization length, as shown in Eq. S3.

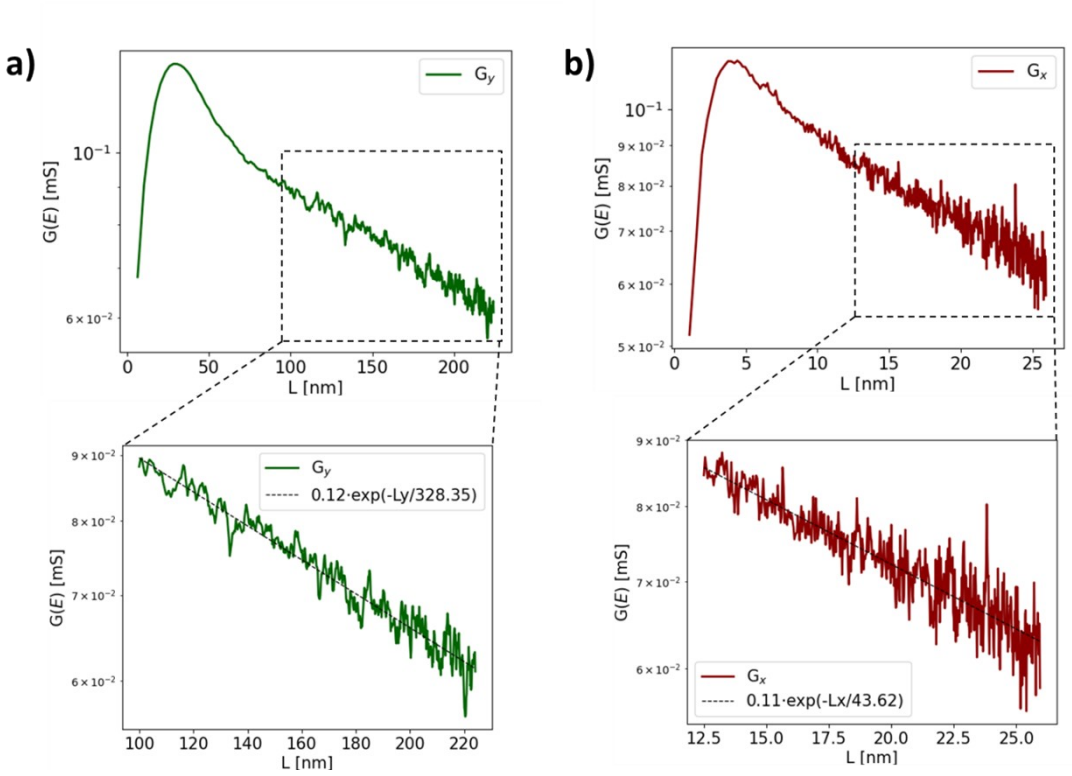

Fig. S5. a) Log-scale plots of $G_y(L_y)$ and b) $G_x(L_x)$ for the para-NPG at E – E_F = 0.4eV and their fit to an exponential decay. Such fitting provides access to the localization length, as shown in Eq. S4.

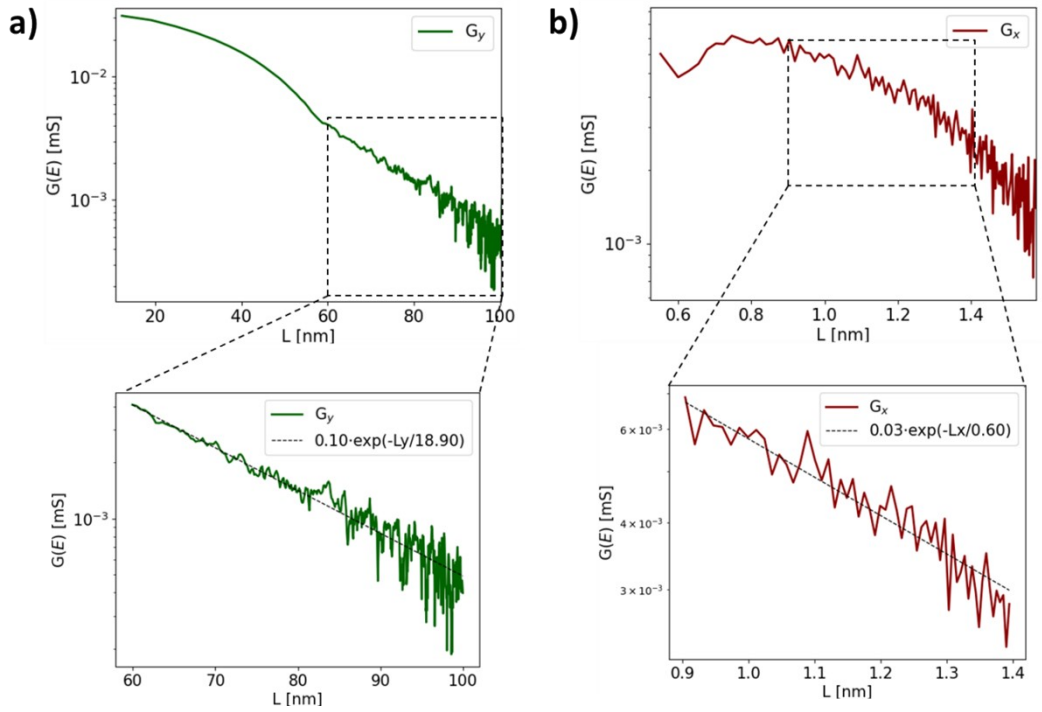

Fig. S6. a) Log-scale plots of $G_y(L_y)$ and b) $G_x(L_x)$ for the meta-NPG at E – E_F = 0.4 eV and their fit to an exponential decay. Such fitting provides access to the localization length, as shown in Eq. S4.

The fits for each NPG allow us to extract the corresponding localization length, $\xi(E)$, for each in-plane direction. With that, in turn, one could calculate anisotropy as ξ_y/ξ_x. Table S2 summarizes these results.

Table S2. Electric anisotropy at E – E_F = 0.4 eV for each material under disorder as characterized by the ratio between localization lengths (ξ_y and ξ_x).

	NPG	para-NPG	meta-NPG*
ξ_y **[nm]**	903.5	328.4	18.9
ξ_x **[nm]**	226.9	43.6	0.6
$A = \frac{\xi_y}{\xi_x}$	4.0	7.5	31.4

Although the ξ_y/ξ_x value for meta-NPG may seem too low (as compared to the $A \approx \infty$ estimation in the main text), it is worth looking at the resulting effect on measurable transport. Using the same fits provided in Figs. S4-6, one may extrapolate the direction-dependent conductance for a given device length. Table S3 provides such extrapolated values for 100x100 nm² devices composed of each NPG. As one may see, the apparently moderate difference in localization lengths for meta-NPG (Table S2) should lead to an extraordinary difference in measurable current for this particular device configuration, clearly supporting the statement that $A \approx \infty$ in

this material. On the contrary, the other NPGs display much lower anisotropy values that are similar to those reported for well-known low-symmetry 2D materials.[3]

Table S3. Conductance values at $E - E_F = 0.4$ eV for all materials under disorder for a 100x100 nm^2 device (G_y^{100nm}, G_x^{100nm}) extracted from their associated strong localization fit (eq. S4). See the legends in Figs. S4-6 for each fitted equation per material. Anisotropy may then be calculated as the ratio between such direction-dependent conductance values.

	NPG	para-NPG	meta-NPG
G_y^{100nm} **[mS]**	0.22	0.09	0.00049
G_x^{100nm} **[mS]**	0.15	0.01	$2.0 \cdot 10^{-74}$
$A = \frac{G_y^{100nm}}{G_x^{100nm}}$	1.44	7.76	$2.48 \cdot 10^{70}$

Section S3: Wave packet propagation lengths

In meta-NPG, the variability of saturation values for L_y between different puddle distributions is apparent for the first 5 ps both at $E - E_F = 0.4$ eV (Fig. 3b in main text) and at $E - E_F = 0.7$ eV (Fig. S7b) and is not present in the other NPGs (see Fig. S8), which highlights it as a consequence of the 1D transport present in meta-NPG. This may be understood by the fact that in NPG and para-NPG transport is more spread through the entire 2D material, thus being more effectively randomized due to scattering with most of the puddles in the sample. Such situations will be less sensitive changes in the particular puddle distribution, and so all puddle distributions give rise to approximately the same wave-packet propagation length profiles (Fig. S8).

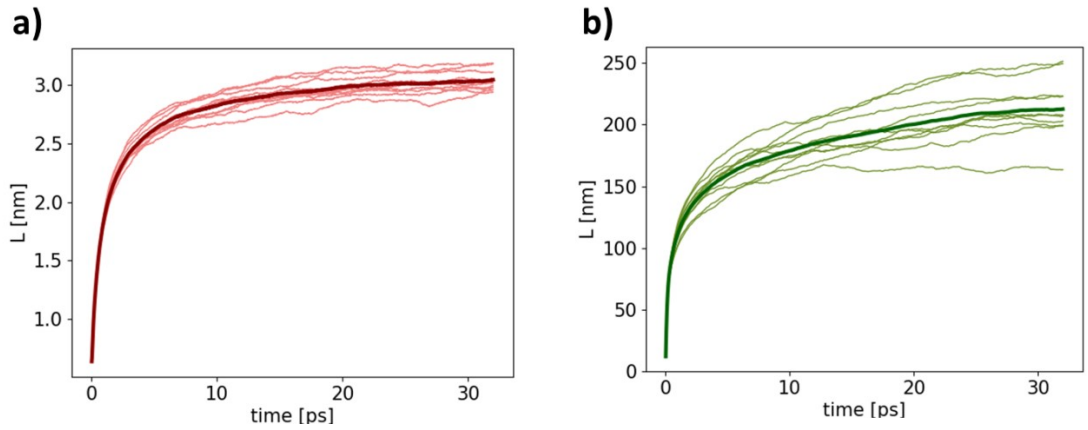

Fig. S7. Time evolution of wave packet propagation lengths for meta-NPG at $E - E_F = 0.7$ eV for different puddle distributions (light curves) and their average (dark curves) along a) the perpendicular direction to GNRs (L_x) and b) parallel to them (L_y).

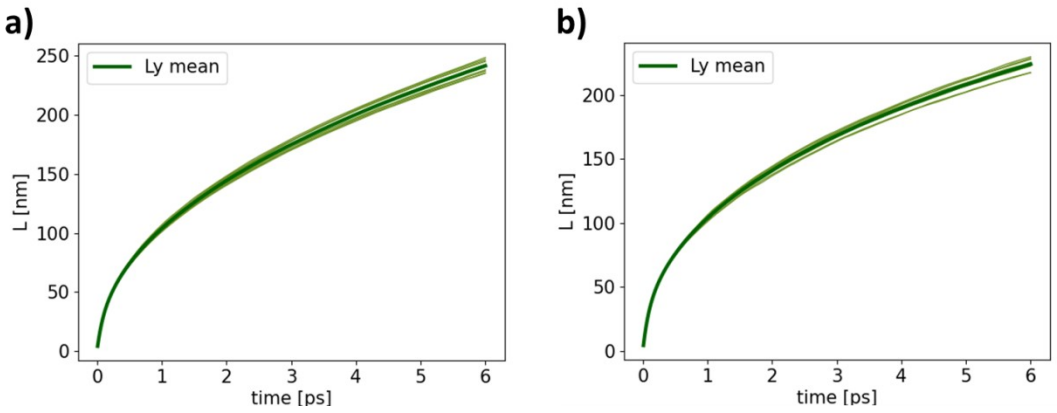

Fig. S8. Time evolution of wave-packet propagation lengths along GNRs (L_y) at E – E_F = 0.4 eV for a) NPG and b) para-NPG for different puddle distributions (light curves) and their average (dark curves).

On the contrary, in meta-NPG transport is restricted within each GNR, which effectively blocks the randomization of the wave-packet by puddles placed at neighbouring GNRs or further away along the x-direction. As a consequence, overall transport is highly sensitive to the specific puddle distributions within each GNR, which makes the transport properties of the entire 2D material far more sensitive to variations in puddle distribution. This leads to different random distributions generating very different conductivity profiles along the GNRs, as may be seen in Fig. 3b in the main text (L_y at E – E_F = 0.4 eV) and Fig. S7b (L_y at E – E_F = 0.7 eV).

Section S4: Effects of puddle concentration and shape

To qualitatively assess how puddle density affects the herein reported giant transport anisotropy of meta-NPG, one may take a look at the wave-packet propagation for varying puddle densities. We here consider 0.01% and 0.5%, with the intermediate density of 0.1% already shown in the main text. The first represents a ten-fold diluted situation as compared to our chosen puddle density (0.1%) whereas the second is five times more concentrated. More diluted puddle distributions (Fig. S9) lead to a slight increase of the wave-packet propagation across GNRs (L_x saturates to 6-7 nm), but they significantly improve transport along GNRs (L_y saturates beyond 1400 nm). Therefore, such diluted disorder increases anisotropy for meta-NPG as compared to 0.1% puddle density. On the contrary, moving to much higher concentrations (0.5%) leads to a significant degradation of transport along the GNRs (Fig. S10) giving rise to a saturation length (L_y) that approaches the scale of the GNR-width. Consequently, for such very disordered situations, giant transport anisotropy strongly decreases (not being giant anymore) – note though that in such scenarios the electrostatic potential of the material has lost entirely almost its underlying periodicity, as may be observed in the corresponding puddle electrostatic map shown in Fig. S10.

Similar to Fig. S9, soft puddles - capturing the electrostatic effect by underlying substrates such as SiO_2[4,5] - increase anisotropy substantially (Fig. S11). This is because transport across GNRs is still limited to ca. 6 nm, whereas the wave-packet along GNRs is barely scattered by such soft electrostatic disorder, not becoming saturated even after some micrometers (see Fig. S11a).

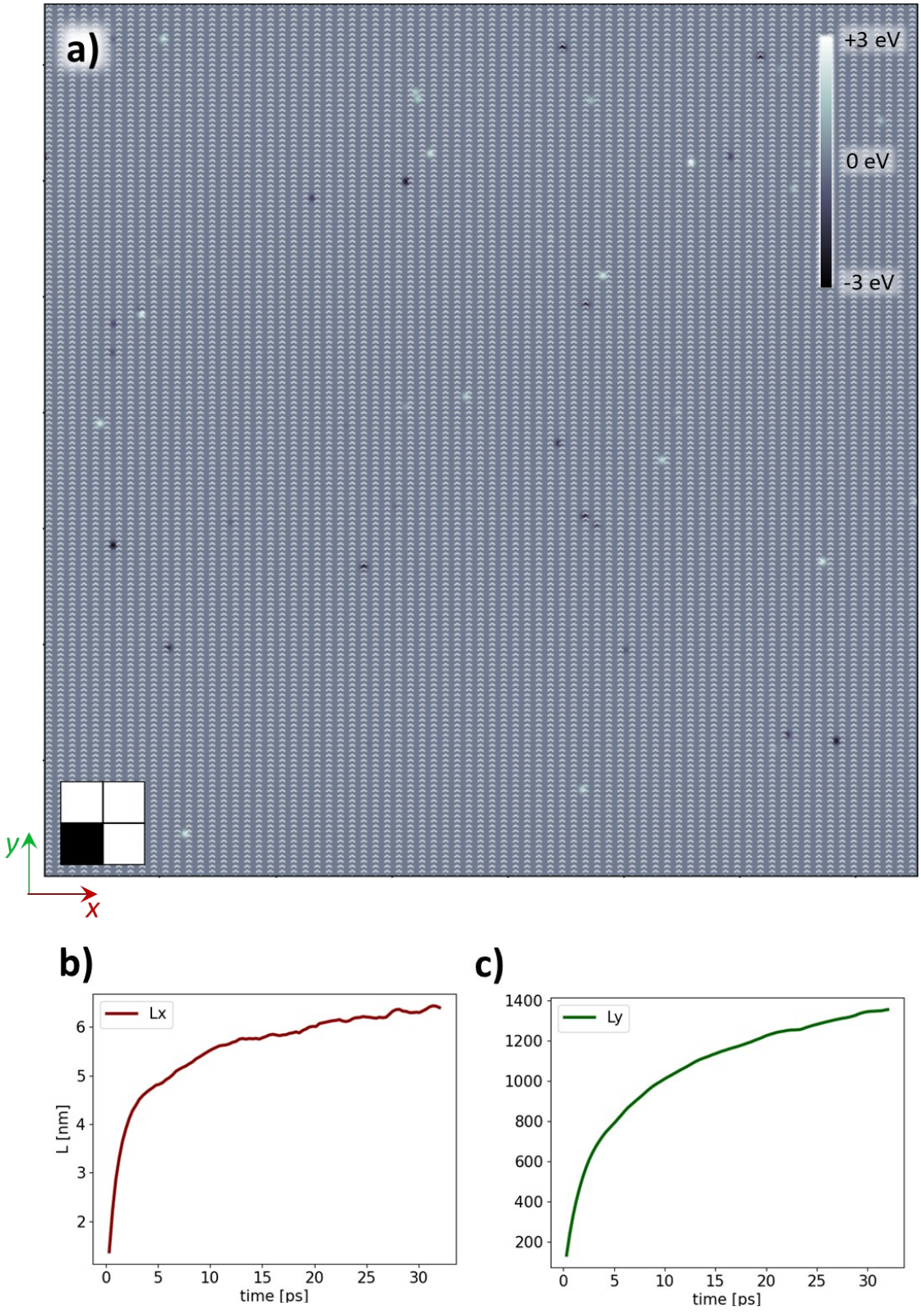

Fig. S9. Results for a puddle density of 0.01%. a) Puddle distribution map for one-fourth of the total area (300x300 nm^2) of the meta-NPG sample (see square outline at bottom left). Bright and dark regions are associated to p-doping ($\varepsilon_i > 0$) and n-doping ($\varepsilon_i < 0$), respectively. Time evolution of wave-packet propagation lengths b) across (L_x) and c) along GNRs (L_y) at E – E_F = 0.4 eV for one puddle distribution.

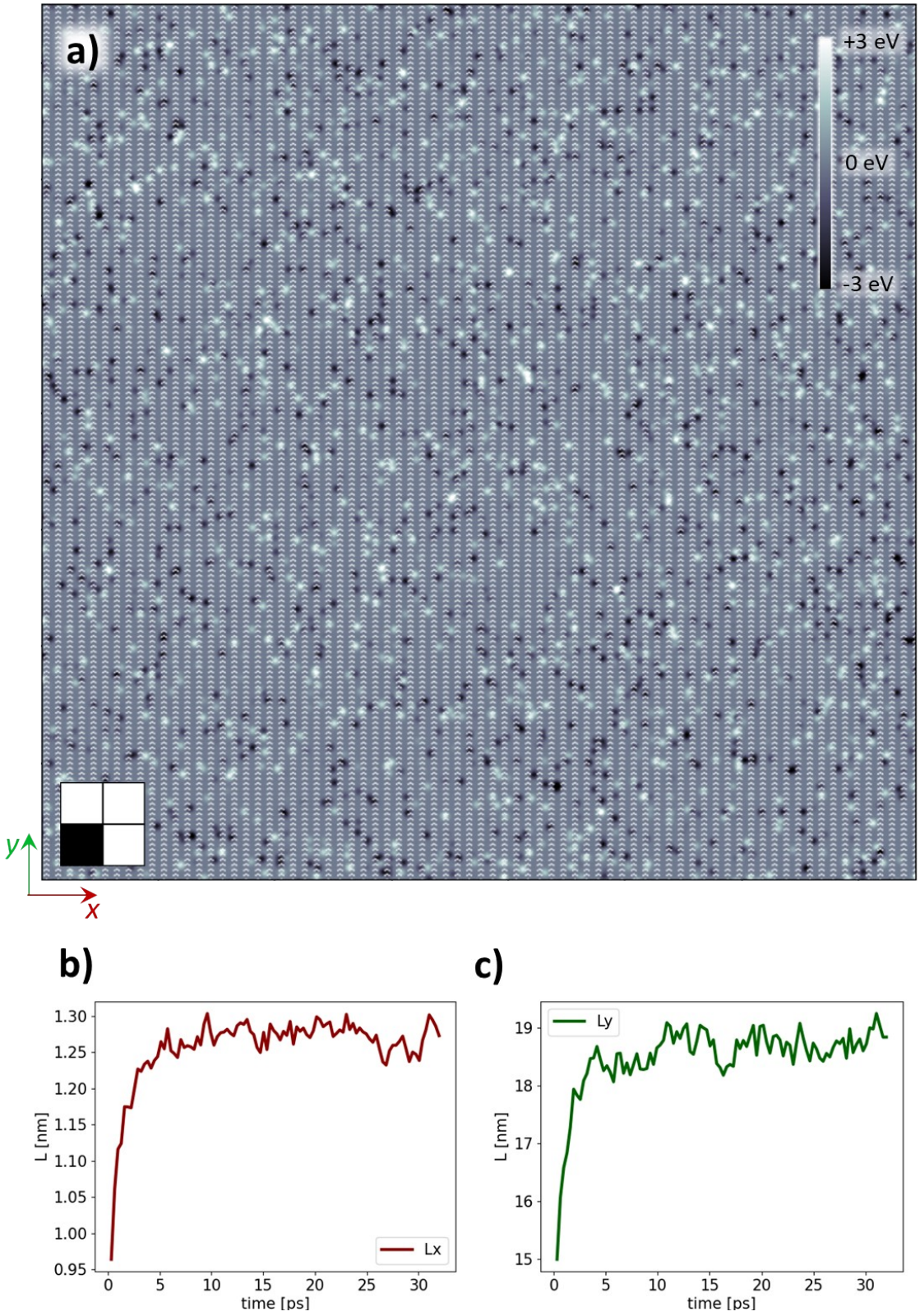

Fig. S10. Results for a puddle density of 0.5%. a) Puddle distribution map for one-fourth of the total area (300x300 nm^2) of the meta-NPG sample (see square outline at bottom left). Bright and dark regions are associated to p-doping ($\varepsilon_i > 0$) and n-doping ($\varepsilon_i < 0$), respectively. Time evolution of wave-packet propagation lengths b) across (L_x) and c) along GNRs (L_y) at E – E_F = 0.4 eV for one puddle distribution.

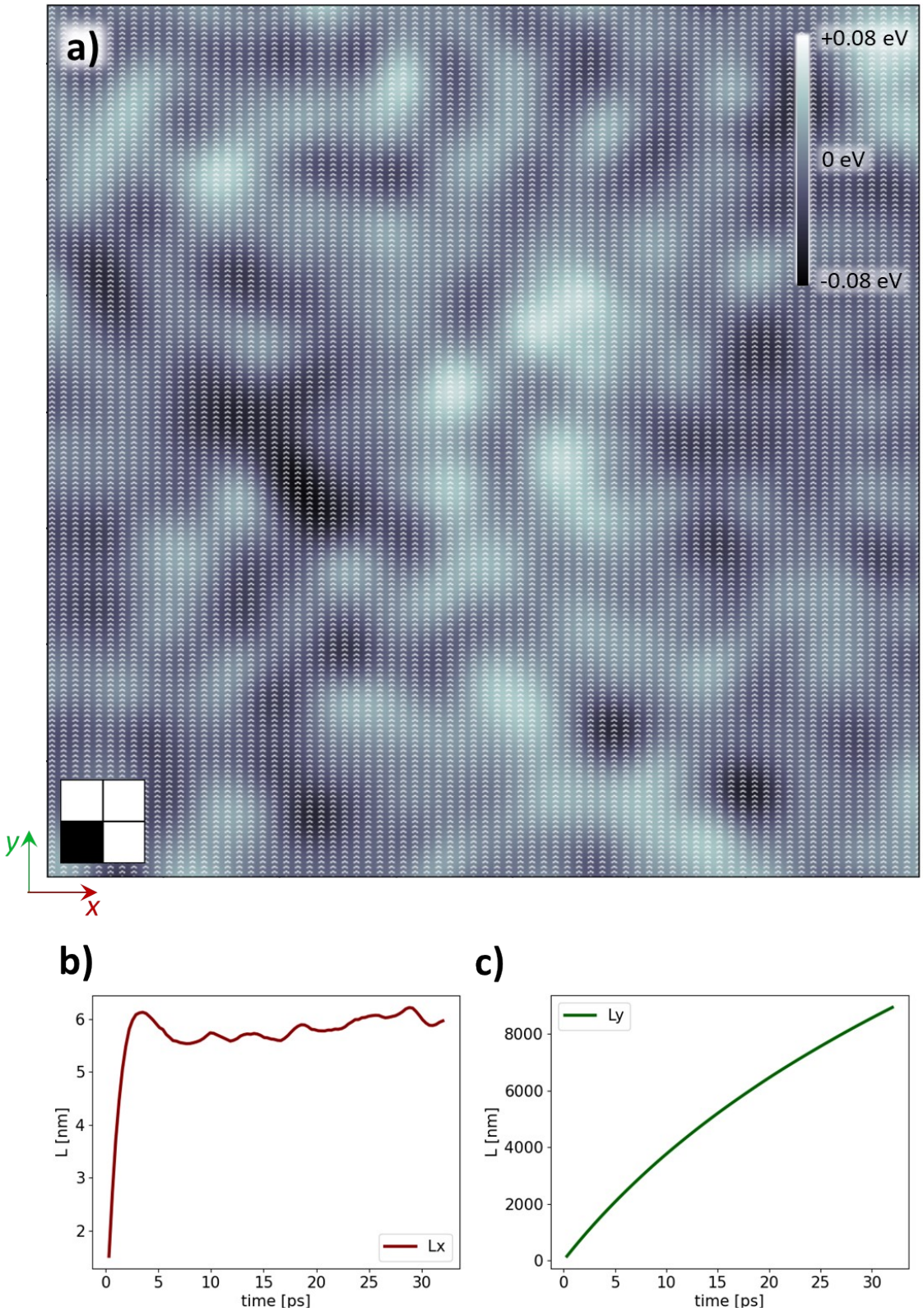

Fig. S11. Results for a puddle density of 0.1% with β = 43.5 Å and Vj ranging from -0.028 and +0.028 eV. These parameters closely resemble the effect of underlying substrates, such as SiO_2.[4,5] a) Puddle distribution map for one-fourth of the total area (300x300 nm^2) of the meta-NPG sample (see square outline at bottom left). Bright and dark regions are associated to p-doping ($\varepsilon_i > 0$) and n-doping ($\varepsilon_i < 0$), respectively. Time evolution of wave-packet propagation lengths b) across (L_x) and c) along GNRs (L_y) at $E - E_F$ = 0.4 eV for one puddle distribution.

Bibliography

1. Papior, N. sisl. https://github.com/zerothi/sisl (2021). doi:10.5281/zenodo.597181

2. Fan, Z. *et al.* Linear scaling quantum transport methodologies. *Physics Reports* **903**, 1–69 (2021).

3. Zhao, S. *et al.* In-plane anisotropic electronics based on low-symmetry 2D materials: Progress and prospects. *Nanoscale Advances* **2**, 109–139 (2020).

4. Martin, J. *et al.* Observation of electron-hole puddles in graphene using a scanning single-electron transistor. *Nat. Phys.* **4**, 144–148 (2008).

5. Deshpande, A., Bao, W., Miao, F., Lau, C. N. & Leroy, B. J. Spatially resolved spectroscopy of monolayer graphene on SiO2. *Phys. Rev. B - Condens. Matter Mater. Phys.* **79**, 205411 (2009).